Available online at www.sciencedirect.com

SciVerse ScienceDirect

Journal of the European Ceramic Society 32 (2012) 441–448

www.elsevier.com/locate/jeurceramsoc

Investigation of ternary system $Pb(Sn,Ti)O_3$–$Pb(Mg_{1/3}Nb_{2/3})O_3$ with morphotropic phase boundary compositions

Dawei Wang [a,b], Maosheng Cao [a,*], Shujun Zhang [b,*]

[a] School of Materials Science and Engineering, Beijing Institute of Technology, Beijing 100081, China
[b] Materials Research Institute, Pennsylvania State University, University Park, PA 16802, USA

Received 1 July 2011; received in revised form 21 August 2011; accepted 25 August 2011
Available online 2 October 2011

Abstract

$(1-x)Pb(Sn_{1-y}Ti_y)O_3$–$xPb(Mg_{1/3}Nb_{2/3})O_3$ ($x = 0.1$–0.4, $y = 0.45$–0.65) ternary system was prepared using two-step columbite precursor method. Phase structure of the synthesized ceramics was studied by using X-ray powder diffraction and the morphotropic phase boundary (MPB) curve of the ternary system was confirmed. The isothermal map of Curie temperature (T_C) in the phase diagram was obtained based on the dielectric–temperature measurements. The coercive field E_C and internal bias field E_i were found to increase with increasing PT content, while decrease with increasing PMN content. The optimum properties were achieved in the MPB composition $0.8Pb(Sn_{0.45}Ti_{0.55})O_3$–$0.2Pb(Mg_{1/3}Nb_{2/3})O_3$, with dielectric permittivity ε_r, piezoelectric coefficient d_{33}, planar electromechanical coupling k_p, mechanical quality factor Q_m and T_C of being on the order of 3040, 530pC/N, 55.5%, 320 and 190 °C, respectively, exhibiting potential usage for high power application.

Keywords: A. Sintering; C. Dielectric properties; C. Piezoelectric properties; C. Ferroelectric properties; $Pb(Sn,Ti)O_3$–$Pb(Mg_{1/3}Nb_{2/3})O_3$

1. Introduction

Lead-based perovskite solid solutions have been widely used in various electronic devices, including piezoelectric actuators, sensors, and acoustic transducers because of their good dielectric and piezoelectric properties.[1–4] Among the lead-based complex perovskites, lead magnesium niobate, $Pb(Mg_{1/3}Nb_{2/3})O_3$ (PMN), is a typical relaxor ferroelectric, exhibiting large dielectric permittivity and a broad diffuse transition near −15 °C.[5] PMN-based binary and ternary systems, such as $Pb(Mg_{1/3}Nb_{2/3})O_3$–$PbTiO_3$ (PMN–PT),[5] $Pb(Mg_{1/3}Nb_{2/3})O_3$–$PbZrO_3$ (PMN–PZ),[6] $Pb(Mg_{1/3}Nb_{2/3})O_3$–$PbZrO_3$–$PbTiO_3$ (PMN–PZ–PT),[7] $Pb(Mg_{1/3}Nb_{2/3})O_3$–$Pb(Sc_{1/2}Nb_{1/2})O_3$–$PbTiO_3$ (PMN–PSN–PT)[8] and $Pb(Mg_{1/3}Nb_{2/3})O_3$–$Pb(Zn_{1/3}Nb_{2/3})O_3$–$PbTiO_3$ (PMN–PZN–PT),[9] exhibit high dielectric permittivity and piezoelectric coefficient with morphotropic phase boundary (MPB) compositions, which is attributed to the enhanced polarizability arising from the coupling between two equivalent energy states, i.e. the tetragonal and rhombohedral phases at MPB, allowing optimum domain reorientation during the poling process.[10,11] Therefore, numerous studies have been focused on the compositions near MPB in different perovskite solid solutions with PMN,[12–15] where good dielectric and piezoelectric properties are expected.

Perovskite compound $PbSnO_3$ (PSn), known to be unstable in the pure form at atmospheric pressure,[16–19] can be stabilized with Ti substitution.[1,17] It was reported that the $PbSnO_3$–$PbTiO_3$ (PSn–PT) binary system showed a behavior analogous to PZT, with good piezoelectric activity near the rhombohedral to tetragonal MPB.[17] Shirasaki et al.[18] prepared PSn–PT solid solution by coprecipitation method and found that the compounds with PT < 0.35 were pyrochlore phase, transforming to Pb_2SnO_4, SnO_2, and perovskite $Pb(Sn_{1-x}Ti_x)O_3$ when fired at 900 °C. Calderón et al.[19] have studied $Na_{0.5}Bi_{0.5}TiO_3$ (NBT) doped PSn–PT with compositions near MPB and found that the addition of NBT decreased the Curie temperature (T_C) of

* Corresponding authors.
E-mail addresses: caomaosheng@bit.edu.cn (M. Cao), soz1@psu.edu (S. Zhang).

0955-2219/$ – see front matter © 2011 Elsevier Ltd. All rights reserved.
doi:10.1016/j.jeurceramsoc.2011.08.038

PSn–PT, with piezoelectric properties changed slightly. Thus, it is desirable to stabilize the perovskite $Pb(Sn,Ti)O_3$ phase and improve the properties by adding various end members. To date, limited work has been carried out to investigate the $Pb(Mg_{1/3}Nb_{2/3})O_3$–$PbSnO_3$–$PbTiO_3$ (PMN–PSn–PT) ternary system. In this work, PMN–PSn–PT ternary ceramics with various PMN and PT levels were synthesized. The phase structure, dielectric, piezoelectric and ferroelectric properties of the ternary system were investigated systematically.

2. Experimental

The PMN–PSn–PT ternary ceramics with compositions of $(1-x)Pb(Sn_{1-y}Ti_y)O_3$–$xPb(Mg_{1/3}Nb_{2/3})O_3$ ($(1-x)Pb(Sn_{1-y}Ti_y)O_3$–xPMN, $x = 0.1$–0.4, $y = 0.45$–0.65) were prepared using two-step columbite precursor method. All the compositions were selected at the proximity of the straight line connecting the two MPBs in PMN–PT and PSn–PT binary systems as shown in Fig. 1.[5,17] The columbite precursor $MgNb_2O_6$ was synthesized at 1000 °C with MgO (99.9%) and Nb_2O_5 (99.9%).[20] Then, Pb_3O_4 (99%), TiO_2 (99.9%), SnO_2 (99.9%) and $MgNb_2O_6$ powders were batched stoichiometrically and wet-milled in alcohol for 24 h. After the slurry was dried, the mixed powders were calcined at 800 °C for 4 h, to synthesis the perovskite compound, subsequently vibratory milled in alcohol for 12 h. The powders were granulated, and pressed to pellets with 12 mm in diameter. Following binder burnout at 550 °C, the pellets were sintered in a sealed crucible containing a $PbZrO_3$ lead source to minimize PbO evaporation at 1200 °C.

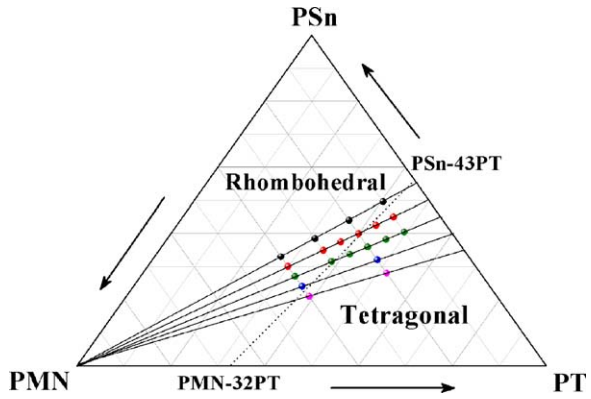

Fig. 1. Phase diagram of $(1-x)Pb(Sn_{1-y}Ti_y)O_3$–xPMN ternary system and composition locations.

The density of the sintered samples was measured using Archimedes method. The phase structure of the sintered samples was studied using X-ray powder diffraction (XRD, PADV and X2 diffractometers, Scintag, Cupertino, CA). For electrical tests, sintered samples were polished parallel using 15 μm SiC powder. Silver paste was printed to form electrodes on both sides of the disc samples and then fired at 700 °C for 10 min. Poling was carried out in silicon oil at 120 °C for 10 min with an electric field of 3 kV/mm. Dielectric measurements were carried out on poled samples using a multi-frequency precision LCRF meter (HP 4184A, Hewlett Packard, Palo Alto, CA). Piezoelectric coefficient was measured on disk samples using a Berlincourt d_{33} meter (ZJ-2, Institute of Acoustics Academia Sinica, Beijing, China). Polarization hysteresis and strain-electric field behav-

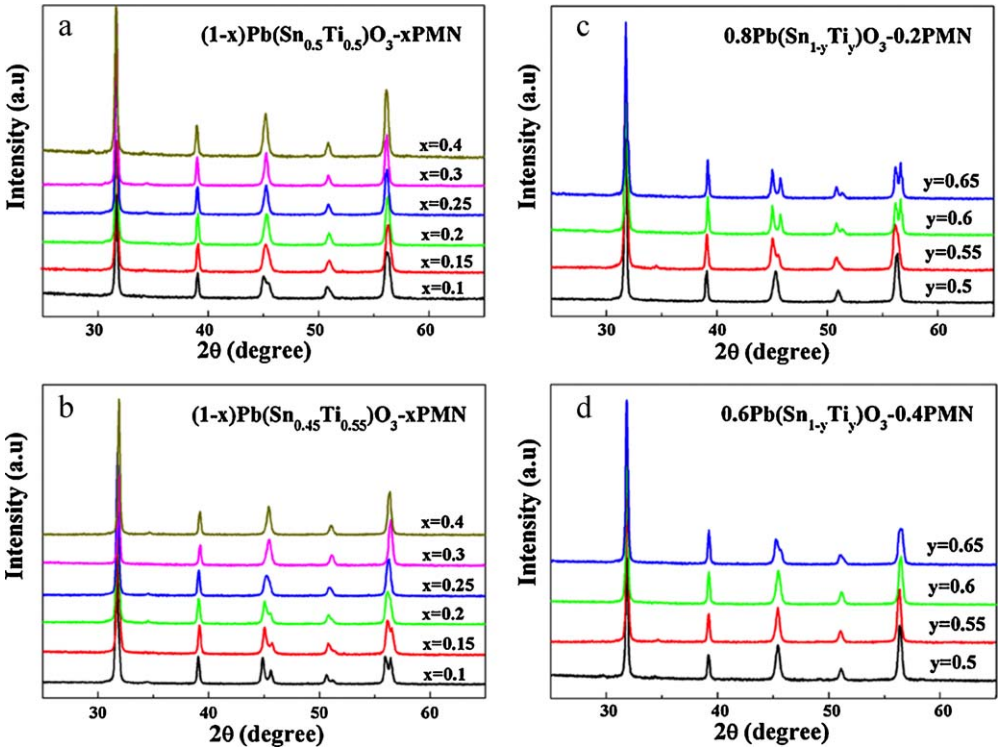

Fig. 2. XRD patterns of $(1-x)Pb(Sn_{1-y}Ti_y)O_3$–xPMN ternary system: (a) $y = 0.5$, (b) $y = 0.55$, (c) $x = 0.2$ and (d) $x = 0.4$.

ior were determined using a modified Sawyer-Tower circuit driven by a lock-in amplifier (Stanford Research System, Model SR830) at a frequency of 1 Hz. The planar electromechanical coupling factor k_p and mechanical quality factor Q_m were determined from the resonance and antiresonance frequencies, which were measured using an Impedance/Gain-phase analyzer (HP 4194A, Hewlett-Packard, Palo Alto, CA) according to IEEE standards.[21,22]

3. Results and discussion

3.1. Structural analysis

The XRD patterns of $(1-x)Pb(Sn_{1-y}Ti_y)O_3$–xPMN with various PMN/PT levels are shown in Fig. 2. It is well known that the typical tetragonal symmetry for perovskite at room temperature is characterized by (2 0 0) peak splitting around $2\theta = 45^\circ$, which was used to determine the MPB compositions, separating rhombohedral and tetragonal phases.[23,24] As shown in Fig. 2(a) and (b), with increasing PMN content, the (2 0 0)/(0 0 2) peaks gradually merge to one peak, indicating the phase transition from tetragonal to rhombohedral phase, where the MPB is found to locate at $x = 0.1$ for $(1-x)Pb(Sn_{0.5}Ti_{0.5})O_3$–$x$PMN and $x = 0.15$–0.2 for $(1-x)Pb(Sn_{0.45}Ti_{0.55})O_3$–$x$PMN, respectively. In addition, with increasing PT content, the splitting of (2 0 0) peak is found to initiate at the composition of $y = 0.55$ for $0.8Pb(Sn_{1-y}Ti_y)O_3$–0.2PMN and $y = 0.65$ for $0.6Pb(Sn_{1-y}Ti_y)O_3$–0.4PMN, respectively, as shown in Fig. 2(c) and (d), indicating that the structure of the ceramics changes from rhombohedral to tetragonal phase, representing the MPB.

According to the XRD results, the approximate MPB curve in the $(1-x)Pb(Sn_{1-y}Ti_y)O_3$–xPMN ternary system is summarized in Fig. 3, including the reported MPBs for PMN–PT and PSn–PT binary systems, being around 68/32 and 57/43.[5,17] The area above this MPB in the PSn/PMN side is in the rhombohedral phase, while that in the lower part with more PT is in the tetragonal phase.

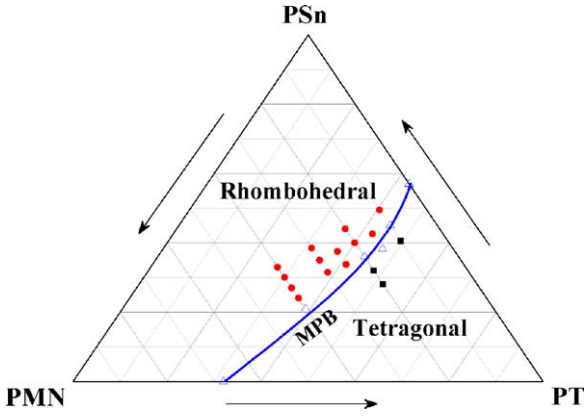

Fig. 3. MPB line for $(1-x)Pb(Sn_{1-y}Ti_y)O_3$–xPMN ternary system: ● rhombohedral phase, ■ tetragonal phase, and △ MPB compositions.

SEM micrographs of the fracture surface for $(1-x)Pb(Sn_{0.45}Ti_{0.55})O_3$–$x$PMN and $0.6Pb(Sn_{1-y}Ti_y)O_3$–0.4PMN with different PMN and PT contents, are shown in Figs. 4 and 5, respectively. It is clearly observed that all samples are highly dense, with a dominating intergranular characteristic. It is found that with increasing PMN content, the grain size of $(1-x)Pb(Sn_{0.45}Ti_{0.55})O_3$–$x$PMN increases significantly, being on the order of 6–10 μm for $x = 0.1$–0.2 and ~15 μm for $x = 0.25$–0.4, as shown in Fig. 4, indicating that the increase of PMN could improve grain growth for PMN–PSn–PT system. In addition, with increasing PT content, the grain size of $0.6Pb(Sn_{1-y}Ti_y)O_3$–0.4PMN is found to vary slightly, being on the order of ~15 μm, as shown in

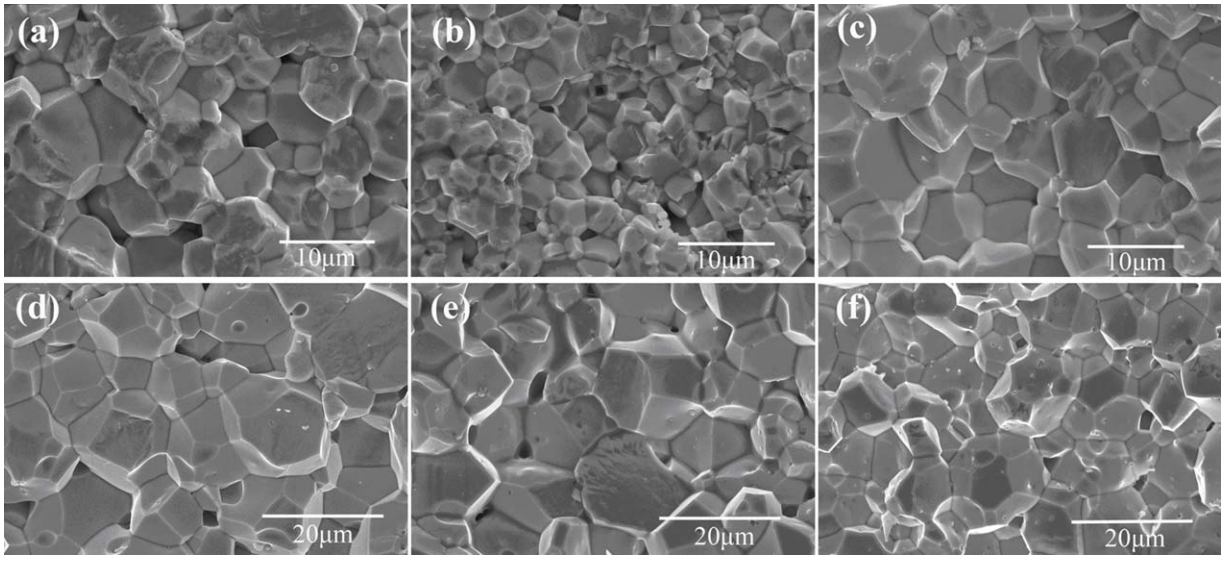

Fig. 4. SEM micrographs of the fracture surface of $(1-x)Pb(Sn_{0.45}Ti_{0.55})O_3$–$x$PMN sintered at 1200 °C: (a) $x = 0.1$, (b) $x = 0.15$, (c) $x = 0.2$, (d) $x = 0.25$, (e) $x = 0.3$ and (f) $x = 0.4$.

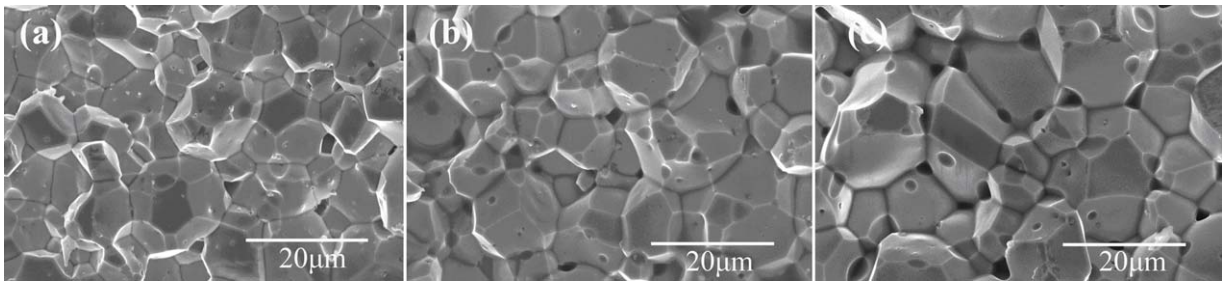

Fig. 5. SEM micrographs of the fracture surface of $0.6Pb(Sn_{1-y}Ti_y)O_3$–0.4PMN sintered at 1200 °C: (a) $y = 0.55$, (b) $y = 0.6$ and (c) $y = 0.65$.

Fig. 5. The average grain sizes for all the studied compositions are listed in Table 1.

3.2. Dielectric properties

The temperature dependence of dielectric permittivity for $(1-x)Pb(Sn_{1-y}Ti_y)O_3$–xPMN with various PMN/PT set levels is shown in Fig. 6 and the dependence of Curie temperature T_C on PMN and PT are shown in Fig. 7. It is clearly observed from Figs. 6(a–c) and 7(a) that with increasing PMN content, T_C gradually decreases from 186 °C to 90 °C, 203 °C to 107 °C and 232 °C to 134 °C for different PT levels of $y = 0.45$, $y = 0.5$ and $y = 0.55$, respectively, which is due to the low maximum transition temperature $T_m \sim -15$ °C of

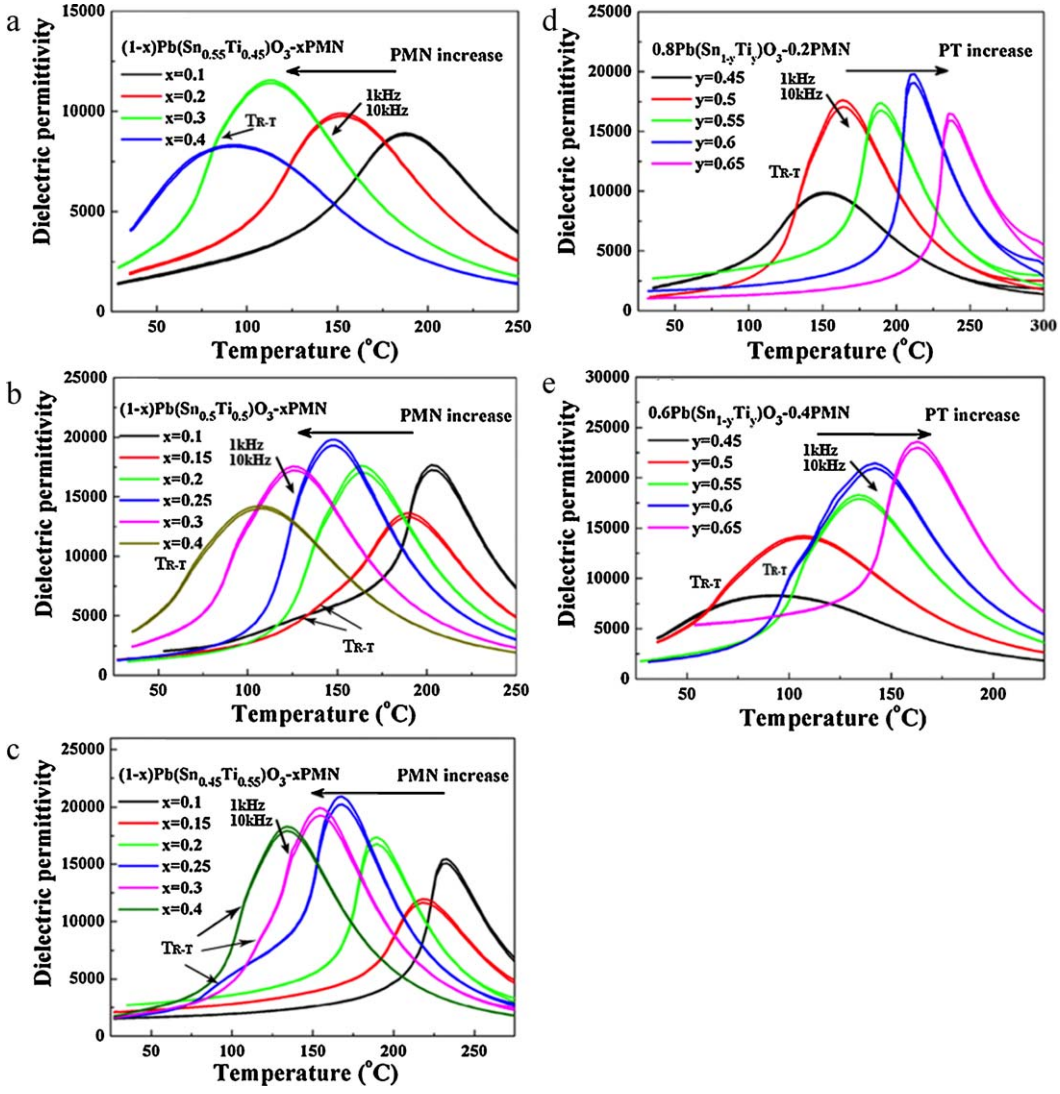

Fig. 6. The temperature dependence of dielectric permittivity for $(1-x)Pb(Sn_{1-y}Ti_y)O_3$–xPMN ternary system: (a) $y = 0.45$, (b) $y = 0.5$, (c) $y = 0.55$, (d) $x = 0.2$ and (e) $x = 0.4$.

Table 1
Dielectric and piezoelectric properties of $(1-x)Pb(Sn_{1-y}Ti_y)O_3$–xPMN ternary ceramics (ρ, density; ρ_r, relative density; G, average grain size; d_{33}, piezoelectric coefficient; k_p, planar electromechanical coupling; Q_m, mechanical quality factor; ε_r, dielectric permittivity; $\tan\delta$, dielectric loss; T_C, Curie temperature; T_{R-T}, rhombohedral to tetragonal phase transition temperature).

$(1-x)Pb(Sn_{1-y}Ti_y)O_3$ –xPMN		ρ (g/cm^3)	ρ_r (%)	G (μm)	d_{33} (pC/N)	k_p (%)	Q_m	ε_r	$\tan\delta$ (%)	T_C (°C)	T_{R-T} (°C)
$y=0.45$	$x=0.1$	8.4	97.7	6	150	23.1	160	1600	3.0	186	–
	$x=0.2$	8.4	97.7	8	80	12.8	220	1800	2.4	151	–
	$x=0.3$	8.4	97.7	14	20	–	–	2500	1.4	112	83
	$x=0.4$	8.3	96.6	15	30	–	–	3900	2.0	90	–
$y=0.5$	$x=0.1$	8.5	98.8	7	420	48.8	220	2040	1.3	203	120
	$x=0.15$	8.3	96.6	8	280	41.1	240	1580	1.4	189	142
	$x=0.2$	8.4	97.7	10	250	39.5	320	1250	1.0	163	140
	$x=0.25$	8.5	98.8	14	180	29.3	200	1480	1.8	147	125
	$x=0.3$	8.4	97.7	15	120	9.2	200	2670	2.0	125	93
	$x=0.4$	8.5	98.8	15	50	–	–	3960	2.2	107	70
$y=0.55$	$x=0.1$	8.5	98.8	6	290	43.8	240	1680	0.7	232	–
	$x=0.15$	8.4	97.7	5	360	47.3	300	2300	0.9	218	–
	$x=0.2$	8.5	98.8	8	530	55.5	320	3040	0.5	190	–
	$x=0.25$	8.4	97.7	15	490	52.7	–	3340	1.2	167	98
	$x=0.3$	8.4	97.7	15	260	33.5	320	2090	1.0	154	120
	$x=0.4$	8.2	95.3	15	50	–	–	2140	1.6	134	108
$y=0.6$	$x=0.2$	8.4	97.7	10	250	39.5	540	1750	0.4	211	–
	$x=0.4$	8.4	97.7	15	280	35.6	70	2240	1.6	142	100
$y=0.65$	$x=0.2$	8.3	96.6	10	140	25.6	570	1100	0.6	236	–
	$x=0.4$	8.4	97.7	16	630	55.7	60	4780	1.2	162	–

PMN; while with increasing PT content, T_C continuously shifts to higher temperature from 151 °C to 236 °C and 90 °C to 162 °C for the content of PMN set as $x=0.2$ and $x=0.4$, respectively, as shown in Figs. 6(d and e) and 7(b), resulting from the high $T_C \sim 490$ °C of PT. Furthermore, as shown in Fig. 6(a–c), with increasing PMN content, the ternary solid solution exhibits more relaxor-like characteristics, showing broadened dielectric peaks and dispersive dielectric behavior with respect to frequency. In addition, the dielectric anomaly prior to T_C for some compositions can be found as shown in Fig. 6, being at the temperature below 150 °C, associated with the rhombohedral to tetragonal phase transition temperature T_{R-T}, as a result of the curved MPB.[5,25] Detailed values of T_C and T_{R-T} for all the compositions are summarized in Table 1.

Based on the above results of dielectric–temperature curve, an isothermal map of T_C for $(1-x)Pb(Sn_{1-y}Ti_y)O_3$–xPMN was developed and plotted in Fig. 8. It is obvious that with compositions approaching PT region, T_C gradually increases, as shown in the isothermal map varying from left to right.

3.3. Ferroelectric properties

Fig. 9(a) shows the bipolar polarization hysteresis and strain electric field loops for $(1-x)Pb(Sn_{0.45}Ti_{0.55})O_3$–$x$PMN as a function of PMN, from which the remnant polarization P_r, coercive field E_C and internal bias field E_i as a function of PMN can be obtained, as given in Fig. 9(b). As indicated, when the PMN content is low, the hysteresis loop of $(1-x)Pb(Sn_{0.45}Ti_{0.55})O_3$–$x$PMN is asymmetric, indicative of high E_i in the ceramics, showing "hardening" characteristics.[26] With increasing PMN content, the hysteresis loop becomes more symmetric, demonstrating the decrease of E_i, as shown in Fig. 9(b). On the other hand, the ferroelectric properties for the compositions of $0.8Pb(Sn_{1-y}Ti_y)O_3$–0.2PMN as a function of PT is shown in Fig. 10. The hysteresis loops are symmetric with low levels of PT, revealing weak E_i in the ceramics. With increasing PT content, the hysteresis loop of $0.8Pb(Sn_{1-y}Ti_y)O_3$–0.2PMN becomes asymmetric, indicating the enhancement of E_i, which is in consistent with the results as shown in Fig. 10(b).

Furthermore, as shown in Figs. 9(b) and 10(b), with increasing PMN/PT content, P_r is found to increase significantly, reaching the maximum value (28.9 μC/cm^2) for the MPB composition $0.8Pb(Sn_{0.45}Ti_{0.55})O_3$–0.2PMN ($x=0.2/y=0.55$), above which P_r decreases, which is due to the coexistence of ferroelectric rhombohedral and tetragonal phases at the MPB compositions. Meanwhile, E_C is found to decrease with increasing PMN content, while increase with increasing PT content, indicating that the domain switching becomes harder with higher PT, resulting from the increase of the tetragonal phase.

3.4. Piezoelectric properties

The dielectric and piezoelectric properties of all the studied compositions for $(1-x)Pb(Sn_{1-y}Ti_y)O_3$–xPMN are listed in Table 1. It is found that the compositions located at the MPB

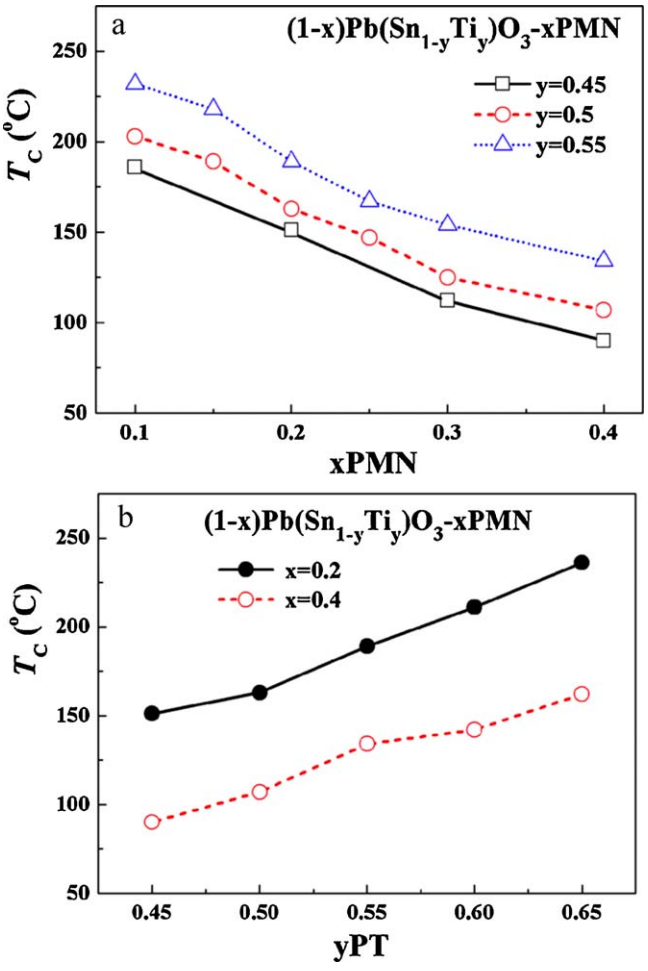

Fig. 7. (a) Curie temperature T_C as a function of PT and (b) Curie temperature T_C as a function of PMN for $(1-x)Pb(Sn_{1-y}Ti_y)O_3$–xPMN ternary system.

curve possess the optimum dielectric and piezoelectric properties with different PT levels, due to the enhanced polarizability arising from the coupling between tetragonal and rhombohedral phases. Furthermore, along the MPB curve moving from PSn–PT side to PMN–PT side, the dielectric permittivity ε_r

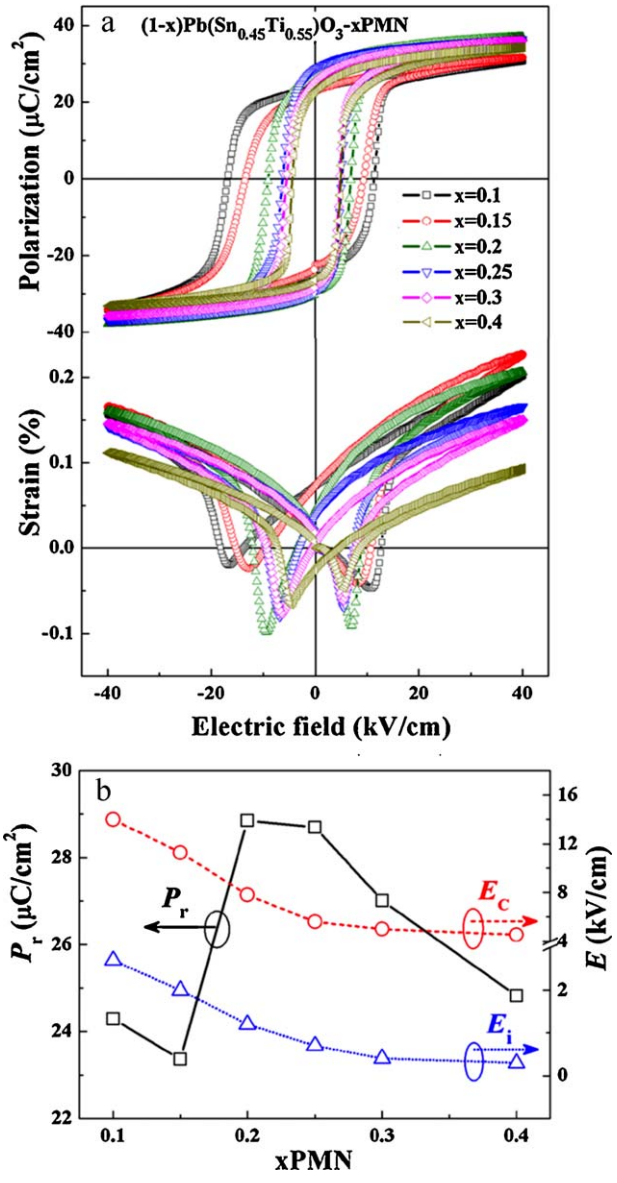

Fig. 9. (a) The bipolar polarization hysteresis and strain electric field loops of $(1-x)Pb(Sn_{0.45}Ti_{0.55})O_3$–$x$PMN and (b) remnant polarization P_r, coercive field E_C and internal bias field E_i as a function of PMN.

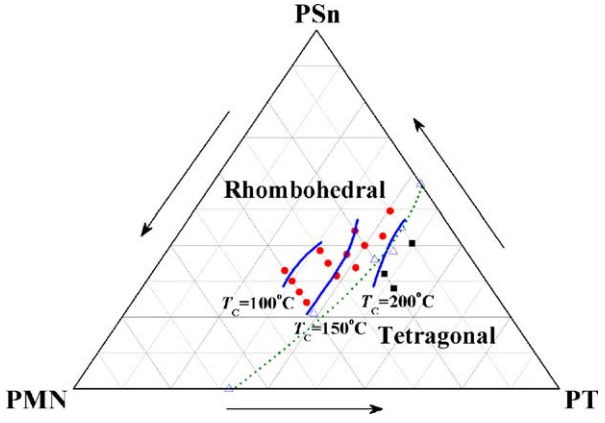

Fig. 8. Isothermal map of the Curie temperature T_C for $(1-x)Pb(Sn_{1-y}Ti_y)O_3$–xPMN ternary system.

and piezoelectric coefficient d_{33} dramatically increase from 2040 and 420pC/N for $0.9Pb(Sn_{0.5}Ti_{0.5})O_3$–0.1PMN to 4780 and 630pC/N for $0.6Pb(Sn_{0.35}Ti_{0.65})O_3$–0.4PMN, respectively, which is mainly attributed to the large ε_r of PMN.[5,15] It should be noted that the high dielectric and piezoelectric properties are achieved at the cost of T_C, with T_C decreasing from 203 °C to 162 °C, resulting from the increase of PMN content (low $T_m \sim -15$ °C). Consequently, for all the compositions studied here, MPB composition $0.8Pb(Sn_{0.45}Ti_{0.55})O_3$–0.2PMN was found to exhibit high dielectric and piezoelectric properties with a moderate T_C, where the ε_r, d_{33} and T_C are on the order of 530pC/N, 3040 and 190 °C, respectively.

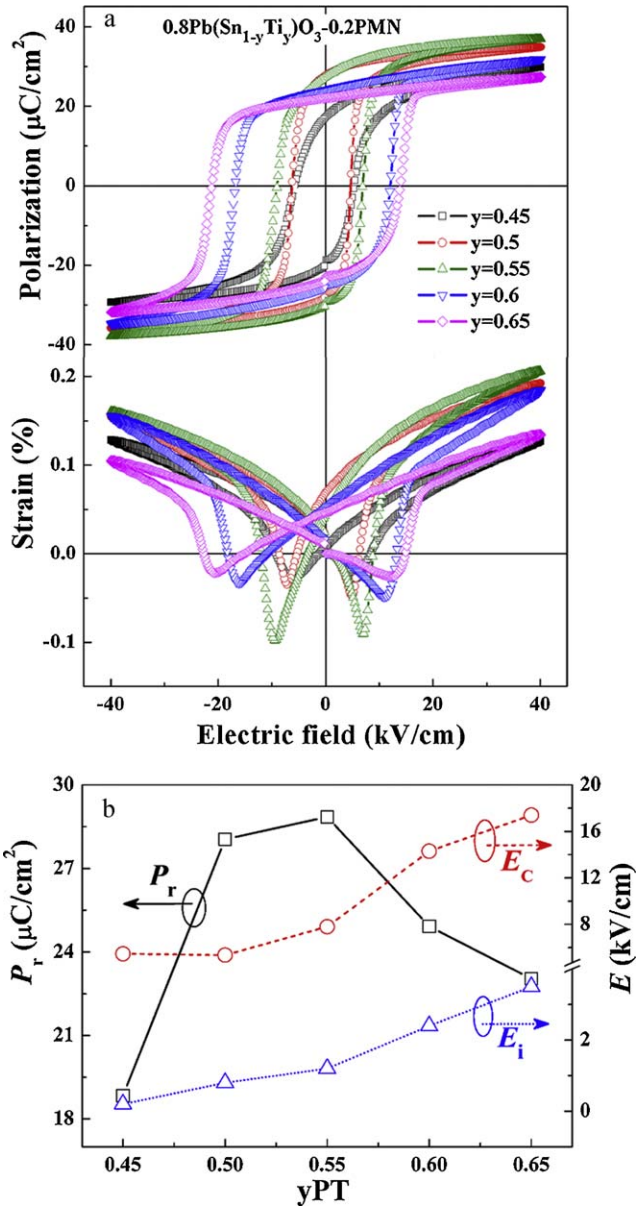

Fig. 10. (a) The bipolar polarization hysteresis and strain electric field loops of $0.8Pb(Sn_{1-y}Ti_y)O_3$–0.2PMN and (b) remnant polarization P_r, coercive field E_C and internal bias field E_i as a function of PT.

4. Conclusions

In conclusion, the $(1-x)Pb(Sn_{1-y}Ti_y)O_3$–xPMN ternary system with compositions near MPB were synthesized using two-step columbite precursor method. Phase structure, dielectric, piezoelectric and ferroelectric properties were investigated systematically. The MPB curve and isothermal map of T_C in the phase diagram for the ternary system were obtained. The optimized composition was found to be the MPB composition $0.8Pb(Sn_{0.45}Ti_{0.55})O_3$–0.2PMN, with ε_r of 3040, d_{33} of 530pC/N, k_p of 55.5%, Q_m of 320, $\tan\delta$ of 0.5%, T_C of 190 °C, P_r of 28.9 μC/cm^2, E_C of 7.9 kV/cm and E_i of 1.2 kV/cm.

Acknowledgements

The authors thank Prof. Thomas R. Shrout for his helpful discussion. Authors from Beijing Institute of Technology acknowledge the National Natural Science Foundation of China under Grant Nos. 50742007, 50872159 and 50972014, and the National High Technology Research and Development Program of China under Grant No. 2007AA03Z103. The author (D.W. Wang) wishes to acknowledge the support from the China Scholarship Council. The work was supported by ONR.

References

1. Jaffe B, Cook WR, Jaffe H. *Piezoelectric ceramics*. London, New York: Academic Press; 1971.
2. Haertling GH. Ferroelectric ceramics: history and technology. *J Am Ceram Soc* 1999;**82**:797–818.
3. Wang DW, Cao MS, Yuan J, Zhao QL, Li HB, Zhang DQ, Agathopoulos S. Enhanced piezoelectric and ferroelectric properties of Nb_2O_5 modified lead zirconate titanate-based composites. *J Am Ceram Soc* 2011;**94**:647–50.
4. Cao MS, Wang DW, Yuan J, Lin HB, Zhao QL, Zhang DQ. Enhanced piezoelectric and mechanical properties of ZnO whiskers and Sb_2O_3 co-modified lead zirconate titanate composites. *Mater Lett* 2010;**64**:1798–801.
5. Choi SW, Shrout TR, Jang SJ, Bhalla AS. Dielectric and pyroelectric properties in the $Pb(Mg_{1/3}Nb_{2/3})O_3$–$PbTiO_3$ system. *Ferroelectrics* 1989;**100**:29–38.
6. Singh G, Tiwari VS. Anomaly in dielectric and piezoelectric properties of $(1-x)Pb(Mg_{1/3}Nb_{2/3})O_3$–$x$PbZrO$_3$ ceramic. *Solid State Commun* 2010;**150**:1778–81.
7. Yoon KH, Lee HR. Electric-field-induced strain and piezoelectric properties near the morphotropic phase boundary of $Pb(Mg_{1/3}Nb_{2/3})O_3$–$PbZrO_3$–$PbTiO_3$ ceramics. *J Appl Phys* 2001;**89**:3915–9.
8. Yamashita Y, Harada K, Tao T, Ichinose N. Piezoelectric properties of the $Pb(Sc_{1/2}Nb_{1/2})O_3$–$Pb(Mg_{1/3}Nb_{2/3})O_3$–$PbTiO_3$ ternary ceramic materials near the morphotropic phase boundary. *Integr Ferroelectr* 1996;**13**:301–8.
9. Gui ZL, Wang Y, Li LT. Lead-based relaxor ferroelectric ceramics for high performance low firing MLCs. In: *Proceedings of the 10th IEEE international symposium on application of ferroelectics*. 1996. p. 409–12.
10. Zhang SJ, Xia R, Lebrun L, Anderson D, Shrout TR. Piezoelectric materials for high power, high temperature applications. *Mater Lett* 2005;**59**:3471–5.
11. Eitel RE, Zhang SJ, Shrout TR, Randall CA, Levin I. Phase diagram of the perovskite system $(1-x)BiScO_3$–xPbTiO$_3$. *J Appl Phys* 2004;**96**:2828–31.
12. Whatmore RW, Molter O, Shaw CP. Electrical properties of Sb and Cr-doped $PbZrO_3$–$PbTiO_3$–$PbMg_{1/3}Nb_{2/3}O_3$ ceramics. *J Eur Ceram Soc* 2003;**23**:721–8.
13. Chen H, Fan C. Fabrication and properties of PYN-PMN-PZT quaternary piezoelectric ceramics for high-power, high-temperature applications. *Mater Lett* 2010;**64**:654–6.
14. Czekaj D, Lisinska-Czekaj A, Kuprianov MF, Zakharov YN. Pyroelectric properties of the multi-component ferroelectric ceramic materials. *J Eur Ceram Soc* 1999;**19**:1149–52.
15. Hou YD, Wu NN, Wang C, Zhu MK, Song XM. Effect of annealing temperature on dielectric relaxation and Raman scattering of $0.65Pb(Mg_{1/3}Nb_{2/3})O_3$–$0.35PbTiO_3$ system. *J Am Ceram Soc* 2010;**93**:2748–54.
16. Sugawara F, Syono Y, Akimoto S. High pressure synthsis of a new perovskites $PbSnO_3$. *Mater Res Bull* 1968;**3**:529–32.
17. Jaffe B, Roth RS, Marzullo S. Properties of piezoelectric ceramics in the solid-solution series lead titanate-lead zirconate-lead oxide: tin oxide and lead titanate-lead hafnate. *J Res Natl Bur Stand* 1955;**55**:239–54.
18. Shirasaki S, Yamamura H, Muramatsu K, Takahashi K. A new pyrochlore system, $Pb(Ti_xSn_{1-x})O_3$, and its transition to a perovskites system. *Bull Chem Soc Jpn* 1974;**47**:1568–72.

19. Calderón F, Portelles J, Siqueiros JM. The variation of the morphotropic zone in $PbTi_{1-x}Sn_xO_3$ ceramics by Na and Bi additions. *Solid State Commun* 1998;**108**:531–3.
20. Swartz SL, Shrout TR. Fabrication of perovskite lead magnesium niobate. *Mater Res Bull* 1982;**17**:1245–50.
21. IEEE standard on piezoelectricity, *ANSI/IEEE Std*. 176-1987. New York: IEEE; 1987.
22. Zhang SJ, Alberta EF, Eitel RE, Randall CA, Shrout TR. Elastic, piezoelectric, and dielectric characterization of modified $BiScO_3$–$PbTiO_3$ ceramics. *IEEE Trans Ultrason Ferroelectr Frequency Control* 2005;**52**:2131–9.
23. Yuan J, Wang DW, Lin HB, Zhao QL, Zhang DQ, Cao MS. Effect of ZnO whisker content on sinterability and fracture behaviour of PZT piezoelectric composites. *J Alloys Compd* 2010;**504**:123–8.
24. Hao H, Zhang SJ, Liu HX, Shrout TR. Dielectric, piezoelectric, and electromechanical properties of morphotropic phase boundary compositions in the $Pb(Mg_{1/3}Ta_{2/3})O_3$–$PbZrO_3$–$PbTiO_3$ ternary system. *J Appl Phys* 2009;**105**:024104.
25. Zhang SJ, Shrout TR. Relaxor-PT single crystals: observations and developments. *IEEE Trans Ultrason Ferroelectr Frequency Control* 2010;**57**:2138–46.
26. Hao H, Zhang SJ, Shrout TR. Dielectric and piezoelectric properties of the morphotropic phase boundary composition in the $(0.8-x)$ $Pb(Mg_{1/3}Ta_{2/3})O_3$–$0.2PbZrO_3$–$xPbTiO_3$ ternary system. *J Am Ceram Soc* 2008;**91**:2232–5.